Earth and Planetary Science Letters 452 (2016) 104–114

Contents lists available at ScienceDirect

Earth and Planetary Science Letters

www.elsevier.com/locate/epsl

Climatic and geomorphic drivers of plant organic matter transport in the Arun River, E Nepal

Bernd Hoffmann [a,*], Sarah J. Feakins [b], Bodo Bookhagen [a], Stephanie M. Olen [a], Danda P. Adhikari [c], Janardan Mainali [d], Dirk Sachse [a,e]

[a] Universität Potsdam, Institut für Erd- und Umweltwissenschaften, Karl-Liebknecht-Strasse 24–25, 14476 Potsdam-Golm, Germany
[b] University of Southern California, Department of Earth Sciences, Los Angeles, CA 90089, USA
[c] Tribhuvan University, Department of Geology, Kathmandu, Nepal
[d] University of North Carolina Wilmington, Department of Geography & Geology, Wilmington, USA
[e] GFZ German Research Centre for Geosciences, Section 5.1, Geomorphology, Potsdam, Germany

ARTICLE INFO

Article history:
Received 22 September 2015
Received in revised form 1 July 2016
Accepted 6 July 2016
Available online 10 August 2016
Editor: D. Vance

Keywords:
plant wax biomarker
leaf wax δD
carbon cycle
remote sensing
erosion

ABSTRACT

Fixation of atmospheric CO_2 in terrestrial vegetation, and subsequent export and deposition of terrestrial plant organic matter in marine sediments is an important component of the global carbon cycle, yet it is difficult to quantify. This is partly due to the lack of understanding of relevant processes and mechanisms responsible for organic-matter transport throughout a landscape. Here we present a new approach to identify terrestrial plant organic matter source areas, quantify contributions and ascertain the role of ecologic, climatic, and geomorphic controls on plant wax export in the Arun River catchment spanning the world's largest elevation gradient from 205 to 8848 m asl, in eastern Nepal. Our approach takes advantage of the distinct stable hydrogen isotopic composition (expressed as δD values) of plant wax *n*-alkanes produced along this gradient, transported in river waters and deposited in flood deposits alongside the Arun River and its tributaries. In mainstem-flood deposits, we found that plant wax *n*-alkanes were mostly derived from the lower elevations constituting only a small fraction (15%) of the catchment. Informed by remote sensing data, we tested four differently weighted isotopic mixing models that quantify sourcing of tributary plant-derived organic matter along the Arun and compare it to our field observations. The weighting parameters included catchment area, net primary productivity (NPP) and annual rainfall amount as well as catchment relief as erosion proxy. When weighted by catchment area the isotopic mixing model could not explain field observations on plant wax δD values along the Arun, which is not surprising because the large arid Tibetan Plateau is not expected to be a major source. Weighting areal contributions by annual rainfall and NPP captured field observations within model prediction errors suggesting that plant productivity may influence source strength. However weighting by a combination of rainfall and catchment relief also captured the observed δD value pattern suggesting dominantly erosive control. We conclude that tributaries at the southern Himalayan front with high rainfall, high productivity, high relief and high erosion rates dominate plant wax exports from the catchment.

1. Introduction

Fixation of atmospheric carbon in terrestrial organic matter and subsequent export into marine basins is one of the key mechanisms responsible for long term carbon burial with a direct impact on global atmospheric CO_2 levels (Berner, 1990; Burdige, 2005). In the Neogene Ganges–Brahmaputra river system, the transfer and burial of organic matter (OM), has been suggested to be more important for atmospheric CO_2 drawdown than the weathering of silicate rocks (France-Lanord and Derry, 1997). Whereas total OM fluxes to marine sinks have previously been estimated using a variety of different methods (France-Lanord and Derry, 1997; Galy et al., 2015, 2011; Goñi et al., 1997; Hedges et al., 1994, 1986; Schlünz and Schneider, 2000; Weijers et al., 2009), other studies have sought to understand the sourcing of OM within large river catchments (Bouchez et al., 2014; Galy et al., 2011; Goñi et al., 2014, 2000; Hedges et al., 2000; Kim et al., 2012; Ponton et al., 2014; Tao et al., 2015). Erosion and geomorphic

* Corresponding author.
E-mail address: hoffmann@geo.uni-potsdam.de (B. Hoffmann).

http://dx.doi.org/10.1016/j.epsl.2016.07.008
0012-821X/

characteristics have been suggested to control catchment scale OM transport (Clark et al., 2013; Galy et al., 2015). But also the significance of runoff for non-petrogenic OM mobilization, in particular triggered by rainstorm events, is increasingly acknowledged (Clark et al., 2013; Hilton et al., 2012; Smith et al., 2013; West et al., 2011). However, climatic and geomorphic drivers are both relevant for organic carbon erosion and mobilization as indicated by several prior studies (Clark et al., 2013; Hilton et al., 2012; Kao and Liu, 1996; Smith et al., 2013; Townsend-Small et al., 2008; Wheatcroft et al., 2010). Specific biomarkers for plants and in particular compound specific isotopic analyses offer promise for tracing plant components of terrestrial organic carbon. In addition, the better identification of source regions and spatial variability of climatic and geomorphic controls on transport processes will allow for a more accurate interpretation of stable isotopic compositions of plant waxes in paleoclimate reconstructions.

Plant-wax lipid biomarkers and their stable isotopic composition (expressed as δD or δ^{13}C value) are established methods to reconstruct paleoclimatic changes from sedimentary archives (e.g. Freeman and Colarusso, 2001; Schefuß, 2003; Tierney et al., 2008). The well-known altitude effect in precipitation isotopes (Dansgaard, 1964; Gonfiantini et al., 2001) has been shown to be recorded in plant wax δD values of living plants (Bai et al., 2011) and in soils (Ernst et al., 2013; Jia et al., 2008). Hence, plant wax δD values have been used in applications tracing vascular plant OM within rivers draining catchments with strong topographic gradients (Galy et al., 2011; Ponton et al., 2014). The resilience of plant waxes makes them a persistent tracer for plant-derived material, whether sourced directly from living plants or after storage in leaf litter and soils. Our approach follows a specific molecule, the C_{29} *n*-alkane, a biomarker for vascular plants. We note that the sources, pathways and fates of other biochemicals with different rates of degradation and different affinities for attachment and packaging with sediments will likely differ (e.g. Hatten et al., 2012; Hedges et al., 2000, 1994). The compound specific approach carries the power and limitations of this specificity within the heterogeneous OM pool. Depending on lithology, sources of *n*-alkanes can include fossil (petrogenic) organic matter (Tao et al., 2015). Studies employing plant waxes in fluvial catchments have revealed novel insights into transport processes: Galy et al. (2011) for example used δD values of plant wax *n*-alkanoic acids extracted from riverine particulate organic matter within the Ganges–Brahmaputra watershed. At the mouth of the Ganges–Brahmaputra, they found the low-elevation plains overwhelmed the contributions from the Himalaya. With more detailed progressive downstream sampling within the Madre de Dios River system in the Peruvian Andes, Ponton et al. (2014) similarly reported plant-wax *n*-alkanoic acid δD values in riverine particulate organic matter and in soils. From the equivalent isotopic gradients in soils and rivers they inferred that this material is representative of its respective catchment, in that fully-forested region. Seasonal contrasts in δD values of riverine particulate organic matter also revealed that during the wet season erosion increased in the higher elevations, which is an equivalent to 1 km higher in the effective catchment sourcing.

While physical erosion has been suggested to be the main driver of particulate organic carbon transport in large river systems worldwide (Galy et al., 2015), no study has yet attempted to assess the relative importance of biomass, climate, and erosional processes within a heterogeneous catchment. In this study, we quantify catchment-wide plant wax contributions from tributaries to the trans-Himalayan Arun River (33,508 km^2), covering a steep altitudinal (Fig. 1A) and climatic (Fig. 1B) gradient (cf. Bookhagen and Burbank, 2006; Olen et al., 2015). Whereas the lower catchment is characterized by tropical to subtropical evergreen forests, the higher Himalaya and the Tibetan Plateau are dominated by sparse alpine vegetation consisting of grasses and shrubs (Fig. 1C, cf. supplement A1 for more details) (Carpenter and Zomer, 1996; Dobremez and Shakya, 1975). We take advantage of the systematic change of plant wax δD (Ernst et al., 2013; Jia et al., 2008; Kahmen et al., 2013a; Peterse et al., 2009; Sachse et al., 2006; Tipple and Pagani, 2013) along altitudinal and hydrological gradients, and make use of it to characterize plant wax δD values along the Arun valley. Together with these observations we employ remote sensing techniques to estimate sourcing of plant-wax *n*-alkane contributions from across the catchment and identify climatic, ecological, and geomorphic drivers responsible for plant wax export from the tributaries.

2. Geographic setting

The Arun River drains the southern Tibetan Plateau (TP) and flows through the eastern Nepalese Himalaya before its confluence with the Tamor and Sun Koshi Rivers in the Siwalik Hills to form the Sapta Kosi (Fig. 1A). The altitudinal range of the catchment extends from 8848 m asl at the summit of Mount Everest to 203 m asl at its outlet into the Sapta Kosi over a horizontal distance of less than 160 km. Downstream, the Sapta Kosi continues ultimately into the Bay of Bengal via the Ganges–Brahmaputra River system. All sampled tributaries drain geological units of either the Greater Himalayan Sequence (late Proterozoic to early Paleozoic paragneisses, calc-silicates and schist) or the Lesser Himalayan Sequence (middle Proterozoic orthogneisses, phyllite, augen-gneiss and quartzite) (Bordet, 1961; Jessup et al., 2008; Quade et al., 2003; Stocklin, 1980). Hence, a contribution of petrogenic plant wax *n*-alkanes is not likely. The TP portion of the Arun catchment is dominated by well-preserved Cambrian to Eocene carbonates and siliclastic sedimentary rocks of the Tethyan Tibetan Zone that potentially contribute petrogenic OM to the Arun, including alkanes such as nC_{29} that are not derived from plant waxes. The plant wax molecular compositions of our samples were used to test this possibility.

The climate of Eastern Nepal is dominated by the Indian Summer Monsoon (ISM) contributing ~70% of the annual rain during its peak season between June and September (Bookhagen and Burbank, 2010). The Siwaliks in the south and the main Himalaya range, including Mount Everest and Makalu, act as orographic barriers to the ISM (Figs. 1B, 2) (Bookhagen and Burbank, 2006). The Tibetan region of the Arun receives very small amounts of rainfall, but additional snow from winter-westerly disturbances originating from the Caspian, Black and Mediterranean Seas (Bookhagen and Burbank, 2010; Lang and Barros, 2004). As a consequence of the climatic and hydrologic conditions, the vegetation in the Arun valley ranges from near-tropical evergreen forests in the south to sparse alpine vegetation in the high altitude part of the valley (Carpenter and Zomer, 1996; Dobremez and Shakya, 1975).

3. Methods

3.1. Sampling

Samples were obtained during two sampling campaigns in September 2011 and October/November 2012, indicated by first two digits of sample ID. River water was sampled at 37 locations (8 mainstem and 29 tributaries; Table 1). Water samples were taken to accompany each of the flood deposit and CPOM samples (see below). They were stored in gas-tight 2 ml glass vials that were flushed before being filled.

Leaves of modern trees and shrubs were sampled at 17 locations along the Arun Valley, at elevations ranging from 87 to 4070 m asl. Sampling of the same C_3 plant species throughout

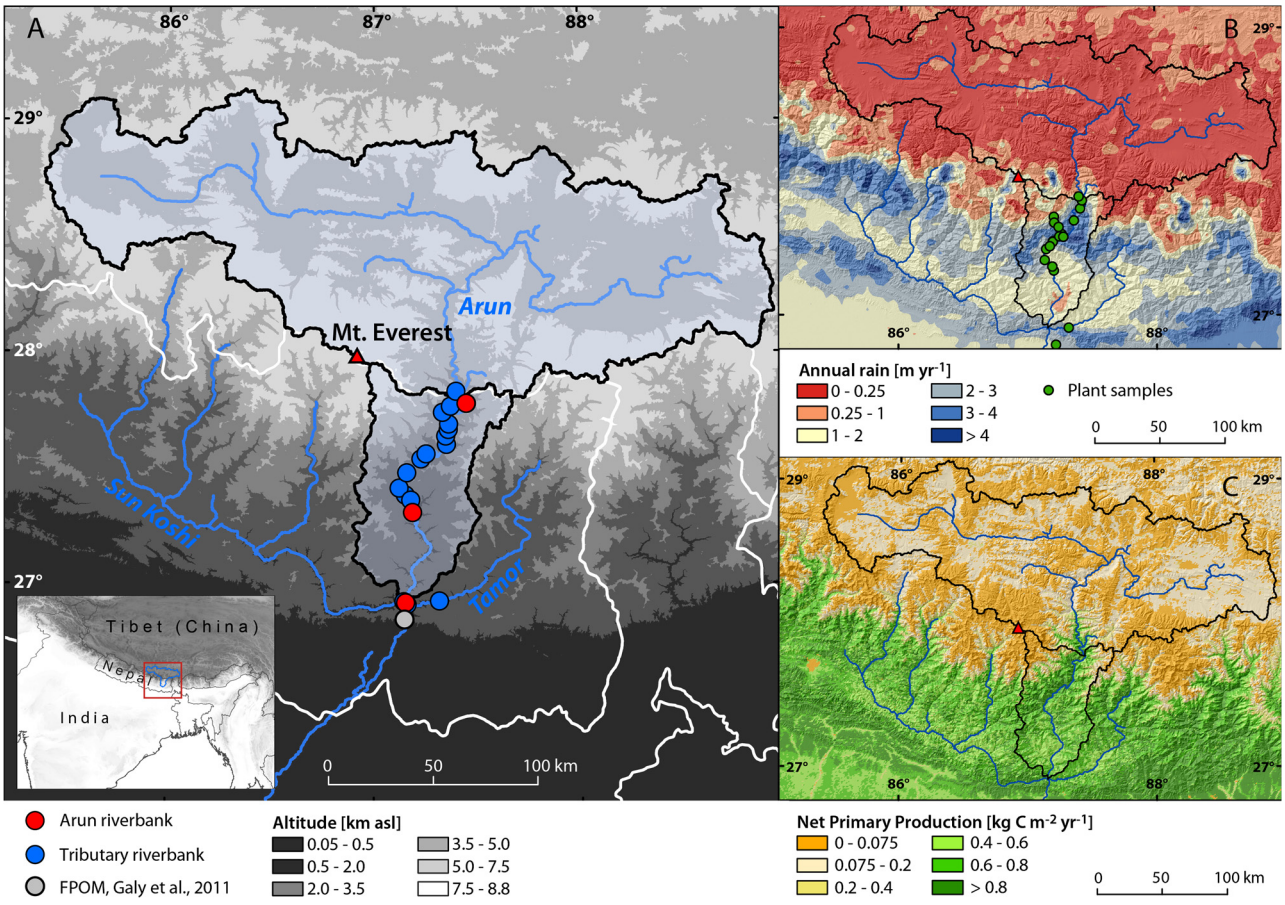

Fig. 1. (A) Topographic map delineating two nested Arun catchments (black lines) above the lowermost and the uppermost mainstem flood-deposit samples (red dots). Tributary flood-deposit sample sites are denoted by blue dots, particulate organic matter sampling by Galy and Eglinton (2011) is shown as grey dot, coarse particulate organic matter (CPOM) samples are not shown here. White lines denote national borders. (B) Mean annual rainfall based on calibrated TRMM 2B31 satellite data (Bookhagen and Burbank, 2010) together with modern vegetation sample sites (green dots). (C) MODIS MOD17A3 Net primary productivity (Running et al., 2004) showing bio-productivity across the catchment.

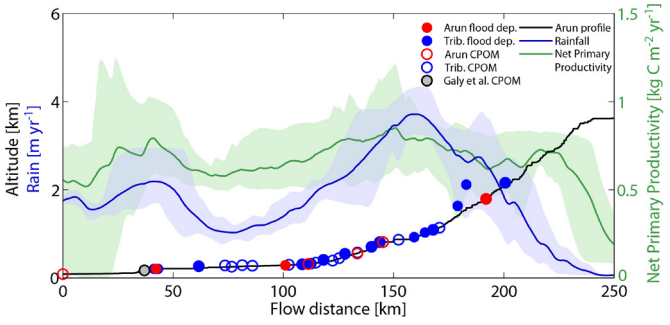

Fig. 2. 50-km wide swath profile of the Arun River (black) from the lowermost CPOM sample site in the Ganges Plain (not shown in Fig. 1) to the Tibetan Plateau with flood deposit and CPOM sample sites. Additionally, net primary productivity (green; Running et al., 2004) and mean annual rainfall rates (blue; Bookhagen and Burbank, 2010) are shown with mean (line) and 5th to 95th percentile (shading).

the catchment was not possible because of ecological turnover of plant communities across the strong climatic gradient. We focus on *Shorea robusta*, a dry-season deciduous or evergreen tree being dominant below 1500 m asl, the widespread evergreen tree *Schima wallichii* and mostly evergreen *Rhododendron spp.* (cf. Table A.1), mostly found at the uppermost sites. At each site three individuals from one to three of the dominant tree species have been sampled, in total 113 individual plants. For each tree, 5–20 mature leaves were randomly sampled from approximately 2 m height, then stored and dried in paper bags.

In total 26 sediment samples of the streams' suspended/bed load material (grain size > 1 mm) were taken (20 × tributaries, 6 × Arun). These samples consist of macroscopic plant debris with varying minor amounts of gravel and are referred to as coarse particulate organic matter (CPOM). In addition, we collected 16 tributary and 3 mainstem flood deposit samples in the immediate proximity of streams less than 1 m above the post-monsoon river level representing seasonal flood deposits of the late ISM discharge (for sampling details, see supplement A2).

3.2. Laboratory methods

3.2.1. Water-isotope analysis

δD values of river water were determined by laser spectroscopy using a Liquid Water Isotope Analyzer (Los Gatos Research, Mountain View, California, USA), at the Institute of Earth and Environmental Sciences, University of Potsdam. Before analysis, samples were filtered through 0.45 µm polyethylene filters. Three standards (−154.3‰, −96.4‰, −9.5‰, Los Gatos Research water isotope standard) were interspersed between every five samples. Out of 6 replicate sample injections, the first three runs were discarded and a mean of the last three measurements was used. To convert sample values to the Vienna Standard Mean Ocean Water (VSMOW)-Standard Light Antarctic Precipitation (SLAP) scale, we used the linear regression function describing the relation between measured and known isotope-standard δD values. Precision is reported as one σ of replicate measurements of the standards, and is 1‰.

Table 1
Sampling locations with stream water δD values and the hydrogen isotopic composition of plant waxes extracted from flood deposits and CPOM (cf. Table A.2 for further details).

Site		Site longitude	Site latitude	Flow distance*	Catchment area (km^2)	Site elevation (m asl)	Catchment med. elev. (m asl)	δD water (‰)	δD water, stdev (‰)	δD nC29 FD (‰)	δD nC29 FD stdev	δD nC29 CPOM (‰)	δD nC29 CPOM stdev
11104	Arun	86.93	26.52	0	57 927.00	87	4543	−90.1	0.2			−174.6	0.5
12151	S.Koshi	87.16	26.91	41	6050.30	205	2351	−69.0	1.4	−187.9	1.3		
12150	Arun	87.15	26.93	42	33 508.00	205	4785	−77.5	0.8	−184.3	1.3		
12149	Tamor	87.15	26.93	43	18 144.00	205	2497	−76.2	0.5	−190.7	3.4		
11090	Tamor	87.32	26.93	62	5884.70	263	2420	−85.8	0.5	−183.8	1.6	−202.1	1.8
11086	Tributary	87.25	27.12	74	83.94	282	1257	−58.5	0.1			−174.7	3.6
11085	Tributary	87.28	27.15	77	90.57	253	1449	−57.6	0.5			−183.8	0.9
11081	Tributary	87.26	27.18	81	35.09	287	1110	−51.7	0.8			−180.7	0.4
11080	Tributary	87.24	27.22	86	314.11	277	1780	−59.7	0.2			−186.0	0.2
12142	Arun	87.19	27.31	101	31 269.00	285	4832	−88.3	0.2	−184.8	3.1		
11075	Tributary	87.18	27.32	103	39.73	298	950	−59.7	0.1			−171.2	1.2
11005	Tributary	87.18	27.37	109	11.35	306	761	−45.9	0.5	−156.6	1.5	−217.2	1.3
11069	Arun	87.16	27.38	111	31 189.00	313	4834	−96.1	0.4			−192.3	2.6
11008	Tributary	87.15	27.39	112	12.21	321	840	−53.9	0.3	−174.5	0.6	−177.9	3.8
11010	Tributary	87.13	27.39	115	74.67	344	1536	−58.5	0.7			−143.4	3.8
11013	Tributary	87.12	27.41	118	205.59	409	1981	−63.0	0.1	−161.1	2.6	−178.1	0.6
11018	Tributary	87.14	27.45	122	351.26	392	2601	−78.5	0.1			−193.1	2.0
11020	Tributary	87.15	27.47	125	3.48	448	1175	−57.5	0.2			−182.6	3.0
11023	Tributary	87.16	27.48	128	11.83	546	1486	−60.0	0.3	−173.2	2.6	−192.3	0.6
11029	Arun	87.19	27.51	134	30 431.00	553	4850	−99.3	0.4			−209.5	1.5
11028	Tributary	87.19	27.51	134	13.28	573	1689	−58.5	0.5			−159.1	0.5
11037	Tributary	87.23	27.54	140	217.53	704	3688	−88.6	0.9	−174.4	1.6	−186.4	1.0
11043	Tributary	87.25	27.57	144	188.28	812	4124	−92.5	0.5	−180.7	5.0	−187.4	1.7
11049	Arun	87.27	27.56	145	29 958.00	812	4858	−105.7	1.1			−183.8	0.3
12009	Arun	87.28	27.57	145	29 958.00	812	4858	−88.7	0.3			−184.6	0.5
12005	Tributary	87.31	27.56	152	82.03	865	2368	−52.2	0.6			−162.8	0.5
12026	Tributary	87.35	27.61	159	165.16	922	3347	−70.9	0.6	−197.0	0.8		
12131	Tributary	87.21	27.68	162	0.09	4000	4044	−81.3	0.3	−225.0	1.7		
12032	Tributary	87.35	27.64	164	9.01	1028	2215	−51.3	0.5	−176.3	0.9		
12129	Tributary	87.21	27.69	164	0.96	4070	4203	−78.2	1.8	−221.7	0.8		
12035	Tributary	87.36	27.67	168	80.30	1090	2780	−65.2	0.5	−185.0	0.7	−184.5	0.7
12043	Tributary	87.36	27.69	171	470.80	1138	4802	−73.7	1.1	−159.8	3.3	−180.5	0.6
12054	Tributary	87.33	27.74	179	28.92	1634	2792	−58.6	0.6	−179.6	3.7		
12063	Tributary	87.37	27.77	183	0.01	2115	2115	−55.9	0.3	−161.2	3.5		
12082	Tributary	87.45	27.78	192	95.43	1787	4097	−84.3	0.4	−188.9	0.9		
12083	Arun	87.45	27.78	192	28 416.00	1793	4878	−109.6	0.7	−206.3	2.0	−176.1	0.6
12097	Tributary	87.40	27.83	201	8.23	2156	3587	−62.8	0.3	−165.2	2.5	−170.9	0.4

* Flow distance upstream lowermost CPOM sample site, cf. Fig. 2.

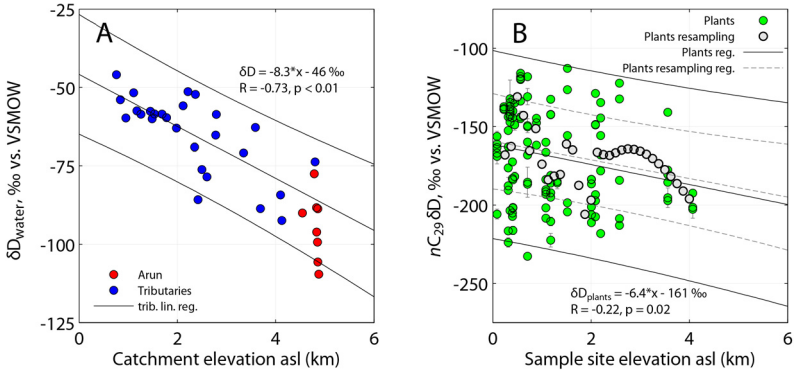

Fig. 3. Isotopic gradients with elevation. (A) Surface water δD values vs. median catchment elevation (analytical precision smaller than dots, cf. Table 1). (B) Plant wax $n\mathrm{C}_{29}$ δD values of modern tree samples, mixed species (each data point is an individual) along the elevation gradient with standard deviation (green points) and resampled $n\mathrm{C}_{29}$ δD values (grey points, 8 samples km^{-1}). Both plots show linear regression and 95% confidence intervals (resampled plant waxes linear regression: $\delta\mathrm{D} = -5.9^{*}\mathrm{x} - 159‰$, $R = -0.44$, $p = 0.01$).

3.2.2. Plant wax extraction and quantification

Flood deposit and CPOM samples were freeze-dried and a total lipid extract (TLE) of the homogenized sample was obtained by extracting the sample on a Dionex ASE 350 accelerated extraction system using 9:1 dichloromethane: methanol. Dried leaf samples were ground and a TLE was obtained using ultrasonic extraction with the same solvent mixture. The aliphatic fraction containing plant-wax *n*-alkanes was obtained through solid-phase extraction. For quantitative and qualitative analysis the purified samples were measured using an Agilent GC MSD (Agilent 5975C MSD, Agilent 7890A GC with Agilent J&W HP-5 ms column, 30 m × 0.25 m × 0.25 µm film) equipped with an additional FID (for a more detailed description of sample processing see Hoffmann et al., 2013).

In order to characterize the samples *n*-alkane distribution, we calculated the average chain length (ACL) using the formula

$$\mathrm{ACL} = \Sigma(\mathrm{C}_n \cdot n)/\Sigma\mathrm{C}_n \quad (1)$$

where n is the number of carbon atoms from 25 to 33 and C_n is the relative abundance. The carbon preference index (CPI) was used to quantify odd over even chain length predominance:

$$\mathrm{CPI} = 0.5 \cdot (\Sigma_{\mathrm{odd}}\mathrm{C}_{25\text{–}31} + \Sigma_{\mathrm{odd}}\mathrm{C}_{27\text{–}33})/\Sigma_{\mathrm{even}}\mathrm{C}_{26\text{–}32} \quad (2)$$

3.2.3. Plant wax isotope analysis

n-Alkane δD values of flood deposits, CPOM and modern leaf samples collected during the 2012 field campaign were measured at the Institute of Earth and Environmental Sciences at the University of Potsdam. Samples taken in 2011 were measured at the University of Southern California. A Thermo Scientific Delta V Plus IRMS coupled to a Trace 1310 GC (Agilent DB-5 column, 30 m × 0.25 mm × 0.25 µm film) via an Isolink pyrolysis furnace operated at 1420 °C was used at Potsdam University. At USC, a Thermo Scientific Trace GC equipped with a ZB-5ms column (30 m × 0.25 mm × 1 µm) was coupled to a Delta V Plus IRMS via an Isolink operated at 1420 °C. δD values obtained on systems at Potsdam University and the University of Southern California were all normalized to the VSMOW-SLAP scale using the same external standard containing C_{16} to C_{30} *n*-alkanes (A-Mix, A. Schimmelmann, Indiana University, Bloomington), run in triplicates after every 6th sample. The overall analytical accuracy of triplicate A-Mix standard analysis was determined to be 3.2‰ (root mean square 0.9‰, $n = 81$). The H_3^+ factor was measured daily and mean values were in the range of 2.99 to 3.37‰ (average = 3.13‰, $\sigma = 0.11‰$). δD values are reported as the mean and 1σ of triplicate measurements.

3.3. Remote sensing topography and climate analyses

Catchment extent and median elevation were determined using a 90-m ground resolution SRTM digital elevation model (DEM) (USGS, 2006) processed with standard Geographic Information System tools (Schwanghart and Kuhn, 2010). As a first-order approximation for erosion rates within the catchment we calculated topographic relief within a 1.5-km radius for each DEM pixel. The distribution of annual rainfall amounts was averaged based on calibrated Tropical Rainfall Measurement Mission (TRMM) satellite data product 3B42 from 1998 to 2010 (Bookhagen and Burbank, 2010); TRMM3B42 data have a 3-h temporal resolution and a 0.25° (~30 km) spatial resolution (Huffman et al., 2007). The Moderate Resolution Imaging Spectroradiometer (MODIS) data product MOD17A3 includes Net Primary Productivity (NPP), a measure for organic matter synthesis reported in grams of carbon per m^2 per year and has a spatial resolution of 1 km (~0.01°). The NPP grid used to approximate land-surface biomass is based on the average of cumulated annual carbon-synthesis rates between 2000 and 2011. We also used MODIS annual mean daytime temperature (MOD11C2, Wan and Dozier, 1996) with the same spatial resolution that is based on 8-day composites. Presented MODIS annual averages are based on 12 yrs of data (2001–2012). In order to characterize stream catchments, raster data were resampled using a bilinear algorithm to match the DEM spatial resolution.

4. Results

4.1. Surface water δD values

Tributaries sampled from 205 to 2156 m asl (median catchment elevations 761 to 4124 m asl) had $\delta\mathrm{D}_{\mathrm{water}}$ values between −45.9 and −92.5‰ (Fig. 3A, Table 1). The relationship between median catchment elevation and tributary $\delta\mathrm{D}_{\mathrm{water}}$ values yielded a slope of $-8.3‰\ \mathrm{km}^{-1}$ ($R = -0.73$, p-value < 0.01). The mainstem Arun River $\delta\mathrm{D}_{\mathrm{water}}$ values decreased with increasing elevation (−78, −88 and −110‰ for catchment median elevations of 4785, 4832 and 4878 m asl, respectively). However, mainstem $\delta\mathrm{D}_{\mathrm{water}}$ values were not linearly correlated to median catchment elevation.

4.2. Plant wax molecular composition

We identified *n*-alkanes in all plant-leaf samples, ranging from 25 to 33 carbon atoms, i.e. chain length, with $n\mathrm{C}_{29}$ and $n\mathrm{C}_{31}$ being dominant (Table A.1). The ACL ranged from 26.9 to 31.6 (mean = 29.1, $\sigma = 1.0$, $n = 113$). CPI values ranged from 0.9 to 22.7 (mean = 6.7, $\sigma = 6$, $n = 113$). Neither plant leaf ACL nor CPI

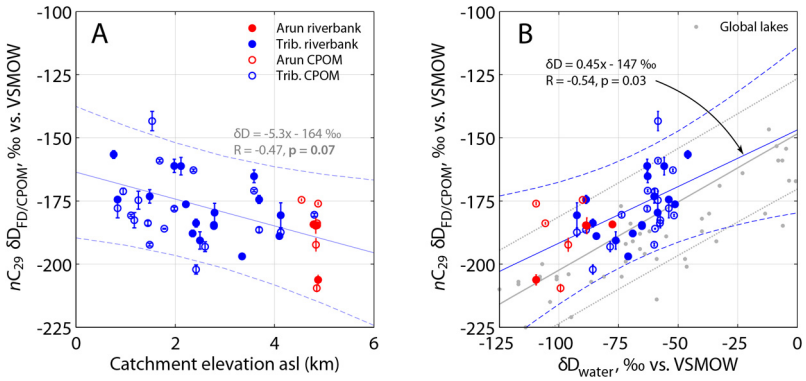

Fig. 4. Isotopic composition of plant waxes in sedimentary samples. (A) Shown versus median catchment elevation, including flood deposit and CPOM samples (this study). Note that linear regression based on tributary flood deposits is not statistically significant ($p = 0.07$). (B) As in part (A) but shown versus δD_{water} values. For comparison data of lake sediments versus mean annual precipitation δD values (grey dots) (Garcin et al., 2012; Polissar and Freeman, 2010; Sachse et al., 2004) with regression ($\delta D_{lake} = 0.55^{*}\delta D_{rain} + 148‰$, grey line).

showed a significant relationship with sample site elevation, annual rainfall amount or NPP. Flood deposit and CPOM samples contained plant wax *n*-alkane distributions that reflect those of plants in the catchment, dominated by nC_{31} and nC_{29} and to a lesser extent nC_{27} (Table A.2). Neither ACL nor CPI of flood deposit and CPOM samples was correlated to catchment median elevation, precipitation or temperature. We do not report absolute abundances of plant wax because we selectively sampled finer deposits when available as we expected them to contain more organic matter than coarser sediments yielding sufficient plant wax for hydrogen isotopic determinations. Thus, our sampling scheme was not designed to quantify flux.

4.3. Plant-wax n-alkane δD values

Plant-wax δD values of living plants (δD_{leaf}) ranged from $-78‰$ (sample 11004-lc1, nC_{29}, *Shorea robusta*) to $-242‰$ (sample 11047-lc3, nC_{31}, *Engelhardtia spicata L.*). The mean nC_{29} δD_{leaf} value was $-168‰$ ($\sigma = 30‰$, $n = 113$). Due to strong variability nC_{29} δD_{leaf} values showed only weak correlation with sample site elevation ($R = -0.22$, $p = 0.02$) with a slope of $-6.4‰\,km^{-1}$ (Fig. 3B). Due to decreasing data density with increasing altitude a spline resampling between 250 and 4000 m asl was conducted with a sampling rate of 8 points km^{-1}. The respective isotopic gradient was $-5.9‰\,km^{-1}$ with an intercept of $-159‰$ ($R = -0.44$, $p = 0.01$, Fig. 3B).

Because of low plant wax abundances in flood deposits only nC_{29}-alkane δD values could be obtained in triplicate for all flood deposit (δD_{FD}) and CPOM (δD_{CPOM}) samples. In 42 samples chain length distributions were sufficient to measure additional compounds. We found nC_{29} δD values to be correlated with nC_{27} δD ($R = 0.72$, $p < 0.01$), nC_{31} δD ($R = 0.69$, $p < 0.01$) and nC_{33} δD values ($R = 0.72$, $p < 0.01$). Hence, we focus on nC_{29} δD values in the subsequent data analysis (see Table A.2 for complete dataset). Regarding tributary flood deposit nC_{29} δD values ($\delta D_{FD,trib}$) we combined the two flood deposit datasets for further analysis. We expect residence times of plant organic matter to be at least several years averaging out a potential interannual variability of synthesized plant wax δD values on the catchment scale. $\delta D_{FD,trib}$ values ranged from $-157‰$ to $-197‰$ ($n = 16$), the linear regression with median catchment elevation yielded a slope of $-5.3 \pm 2.7‰\,km^{-1}$, but was not significant within 95% confidence intervals ($R = -0.47$, $p = 0.07$) (Fig. 4A). 2011 ($n = 16$) and 2012 ($n = 4$) CPOM data were also combined. $\delta D_{CPOM,trib}$ values ranged from $-217‰$ to $-145‰$ (median $= -182‰$, $n = 20$), and were not correlated to median catchment elevation. Arun mainstem CPOM δD values were within the same range as observed for tributaries and ranged from $-210‰$ to $-175‰$ ($n = 6$), but like tributaries showed no trend with elevation. A comparison of tributary δD_{FD} values with the isotopic composition of surface water (Fig. 4B) yielded a significant linear relationship, with $\delta D_{FD} = (0.45 \pm 0.19)^{*}\delta D_{water} - 147 \pm 13‰$ ($R = 0.54$, $p = 0.03$), but the relationship was not significant for CPOM samples ($R = 0.24$, $p = 0.33$). The three Arun mainstem flood deposits saw a downstream D-enrichment from $-206‰$ to $-184‰$. We calculated the isotopic enrichment between mainstem *n*-alkanes sampled at the highest (Tibetan Plateau, TP) and the lowest (Himalayan Range, HR) location ($\varepsilon_{HR/TP}$) to be $+27‰$ using the equation:

$$\varepsilon_{HR/TP} = \left(\left(\delta D_{FD,TP} + 10^3\right)/\left(\delta D_{FD,HR} + 10^3\right) - 1\right) \cdot 10^3 \quad (3)$$

4.4. Remote sensing data

TRMM 3B42 satellite-rainfall data indicate that only 34.7% of the Arun's annual rainfall occurs in the upper 84.8% of the catchment (north of the Nepal–China border) whereas, the majority, 65.3%, is received in the lower 15.2% (between the border and the Arun/Tamor/Sun Koshi confluence). Rainfall peaks at the southern front of the Siwalik Hills (up to 4 $m\,a^{-1}$) and the main Himalayan range (locally >5 $m\,a^{-1}$), in between locally dropping to less than 1 $m\,a^{-1}$ (Figs. 1B, 2). MODIS-derived annual mean NPP values follow rainfall distribution: they increase at the southern front of the Siwalik Hills and remain constant until the southern front of the main Himalayan ranges, beyond which NPP drops on the TP as rainfall decreases (Figs. 1C, 2).

5. Discussion

5.1. Elevation gradients in precipitation and stream water isotopic composition

A negative correlation between precipitation isotope ratios and elevation is expected based on the altitude effect (Dansgaard, 1964). For late to post ISM stream waters of the Arun's tributaries, we found a gradient of $-8.3‰\,km^{-1}$ (using catchment median elevation, $\sigma = 1.6‰\,km^{-1}$) and of $-8.8‰\,km^{-1}$ (using mean elevation, $\sigma = 1.5‰\,km^{-1}$), which is within the observed range of gradients of precipitation δD values with elevation in the tropics worldwide (Gonfiantini et al., 2001). It is also comparable to gradients found along other rivers at the southern TP margin after re-evaluating data for comparable elevation ranges, e.g. the Lower Yarlung Tsangpo, Po Tsangpo and Siang Tsangpo Basins in the eastern Himalaya (Hren et al., 2009) and the Kali Gandaki

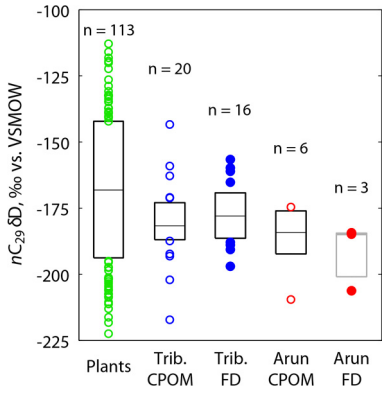

Fig. 5. Box plots showing nC_{29} δD values of living plants, mainstem and tributary CPOM and flood deposits across the entire transect. Boxes denote 25th and 75th percentile range, median (line) and outliers (circles).

River (Garzione et al., 2000). Even though the relationship between altitude and stream water δD values might vary throughout the year it represents our best estimate of the D-depletion of precipitation with increasing altitude in the Arun valley, and is consistent with regional observations. The apparent steeper isotopic gradient of mainstem waters was expected due to the very pronounced altitude effect across the orographic front with a strong enrichment of tributary waters south of the main Himalayan axis (Rowley and Garzione, 2007). Additionally, the spatially inhomogeneous rainfall in the Arun with a higher specific runoff south of the main Himalayan ranges enhances the enrichment of Arun mainstem water. The complex hydrology of large-scale river systems with significant temporal storage of precipitation may have also contributed to the steep increase of mainstem δD_{water} values downstream the Arun (Andermann et al., 2012; Bookhagen, 2012).

5.2. Plant wax δD values in Arun tributaries

We find the largest variability in modern plants, when comparing the range of isotopic compositions (75th percentile–25th percentile) in measured samples from living plants (83‰), CPOM (44‰) and flood deposits (35‰) (Fig. 5). Similar patterns have been observed when comparing modern catchment vegetation with lake sediments elsewhere (Hou et al., 2007; Sachse et al., 2006). Despite the high variability between plant individuals and species, we find comparable isotopic gradients for modern plants (-6.4‰ km^{-1}) and flood deposits in tributaries (-5.3‰ km^{-1}). This suggests that flood deposits on the tributary scale represent an integrated sample of plant waxes from their catchments, and is consistent with the findings of Ponton et al. (2014) based on particulate OM sampled in the Peruvian Andes.

While deposition of flood deposits occurs primarily during or just past the ISM season, mobilized upstream material likely integrates over years or decades as plant detritus accumulates as leaf litter and in soils. Tributary contribution of petrogenic plant waxes is unlikely as tributaries along the sampling transect drain catchments characterized by high-grade metamorphic rocks lacking organic matter. This argument is supported by three additional observations: first, observed tributary flood deposit CPI values (mean CPI = 8.4) are much closer to modern angiosperm CPI (~11, Bush and McInerney, 2013) than to petrogenic CPI (typically ~1). Second, mainstem flood deposit CPI is constant along the sampled transect, indicating no significant input of petrogenic n-alkanes with CPI of ~1. Third, Galy and Eglinton (2011) determined the age of nC_{24-32} alkanoic acids extracted from particulate organic matter of the Sapta Koshi watershed (Fig. 1) and found their average age to be 50 yrs BP (cal. ^{14}C age), indicating short residence times for plant waxes in the watershed. Taken together, these indications suggest that the n-alkanes measured in our samples were also derived from recent plant inputs, although this component has not been directly dated.

CPOM, consisting of macroscopic, undegraded plant debris, showed δD values with reduced variability compared to δD_{leaf} indicating integration across a greater number of individual plants and species across the catchment. However, tributary CPOM δD values ($\delta D_{CPOM,trib}$) showed no significant correlation with δD_{water} values, implying that the catchment area is not evenly represented by CPOM. Instead, it is conceivable that CPOM was biased towards vegetation at the rivers' edge as the discharge regime during the late to post-ISM phase is discriminating CPOM export from the tributaries' hill slopes. As a consequence of potentially biased CPOM sourcing we used flood deposit δD_{wax} values for the evaluation of tributary contributions to the mainstem in section 5.3.

5.3. Fluvial integration of plant waxes

Mainstem flood deposits were characterized by a downstream increase of δD_{FD} values (Fig. 6B) due to inflow from lower elevation tributaries. The effect of tributary plant waxes on the mainstem signal is dominated by two factors: the isotopic composition of tributary plant waxes and its quantities. The latter is expected to be a function of catchment characteristics, including biomass productivity and erosion rates. Since climate, plant cover, and erosion vary along the steep Himalayan passage of the Arun, we do not expect uniform spatial integration across the entire catchment, in contrast to tributaries (this study and Ponton et al., 2014). In order to evaluate plant wax sourcing, we model contributions based on linear weighting of catchment size, biomass productivity, runoff and a proxy for erosion. To test the four weighting approaches we combine them with tributary δD_{wax} value estimates for a mass-weighted isotope mixing of mainstem and tributary plant wax n-alkanes and compare predicted vs. measured downstream mainstem δD_{FD} values.

5.3.1. Estimating $\delta D_{FD,trib}$ values for Himalayan tributaries of the Arun River

We sampled 16 accessible tributaries between 205 and 1793 m river elevation and report measured $\delta D_{FD,trib}$ values (Table 1, Fig. 6a). Since the elevation to $\delta D_{FD,trib}$ relationship was not significant at the 95% confidence level ($R = -0.47$, $p = 0.07$, $n = 16$, Fig. 4A) we aimed for a more precise relation in order to predict $\delta D_{FD,trib}$ values along the sampled transect. Therefore, we tested a multi-parameter approach that indirectly accounts for climatic and plant physiological drivers that affect δD_{leaf} values. We account for plant source water by including mean annual temperature (MAT) and elevation (Dansgaard, 1964; Garzione et al., 2000; Rowley et al., 2001), and for plant water evapotranspiration by including MAT and annual rainfall rates (MAP) (Feakins and Sessions, 2010; Kahmen et al., 2013a, 2013b). As such, we set up a system of linear equations, where sampled tributary $\delta D_{FD,trib}$ values are described as a function of elevation, MAP and MAT of respective catchments:

$$\delta D_{FD,trib,1} = x_1 alt_1 + x_2 MAP_1 + x_3 MAT_1 + x_4$$
$$\delta D_{FD,trib,2} = x_1 alt_2 + x_2 MAP_2 + x_3 MAT_2 + x_4$$
$$\cdots$$
$$\delta D_{FD,trib,n} = x_1 alt_n + x_2 MAP_n + x_3 MAT_n + x_4 \quad (4)$$

where alt_n, MAP_n and MAT_n represent tributary catchment median estimates of altitude, annual rainfall and mean temperature ($n = 16$). The system of linear equations was numerically

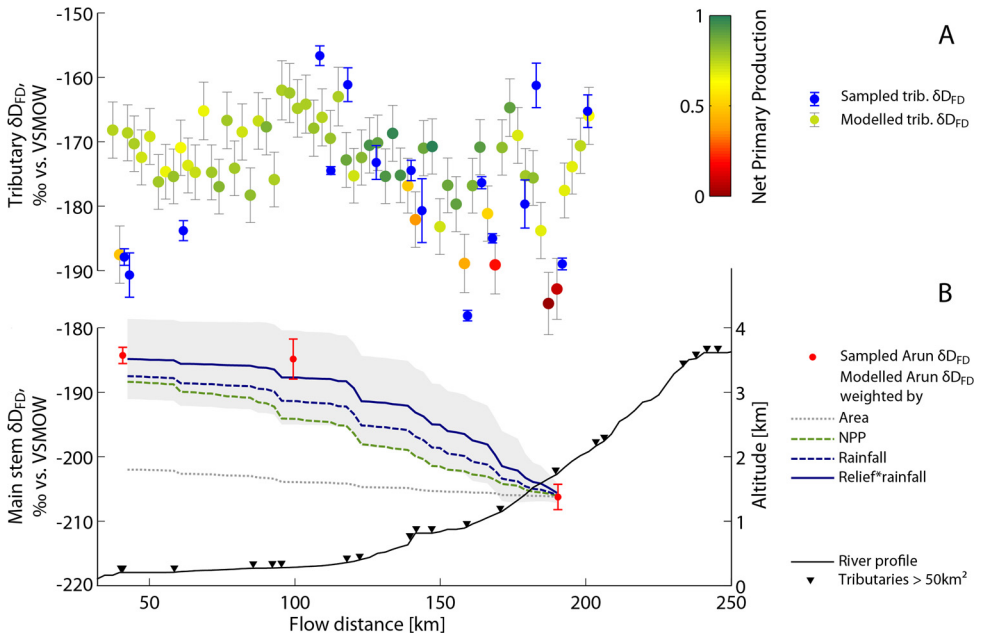

Fig. 6. Modeling plant wax sources. (A) Tributaries. Modeled flood deposit $\delta D_{FD,trib}$ values with 95% CI (blue circles) and measured $\delta D_{FD,trib}$ values (error bars indicate 1σ of triplicate measurements, color indicates mean catchment NPP). (B) Arun mainstem. Comparison of model $\delta D_{FD,Arun}$ estimates with mixing proportions of TP and HR sources weighted by catchment size (grey dotted line), NPP (green dashed line), rainfall (blue dashed line) and by rainfall combined with the local relief (blue solid line). Prediction errors are shown for the *erosion-runoff model* only (grey shading, see supplement A4 for error propagation). All models except for area fall within the error envelope of this model. Measured $\delta D_{FD,Arun}$ values are denoted as red circles (error bars as in A). Triangles along river profile (black line) indicate confluences with largest tributaries.

solved with $x = (-0.0187\ \ -2.4308\ \ -0.0018\ \ -94.06)$. The multi-parameter model solution yielded a much better correlation with observed $\delta D_{wax,trib}$ values ($R = 0.73$, $p < 0.01$) (cf. supplement A3) and was consequently used to obtain tributary $\delta D_{FD,trib}$ value estimates. Resulting $\delta D_{FD,trib}$ values (Fig. 6A) largely reflect rainfall amount (cf. Fig. 2) and the tributaries' median elevation along the Arun. The three samples from the Tamor (2×) and Sun Koshi Rivers draining the High Himalaya (Fig. 6A, tributaries at 42, 43, and 62 km flow distance) are reflected well by the estimated $\delta D_{FD,trib}$ value at the three rivers' confluence at 41 km flow distance.

5.3.2. Mixing models for sourcing within the Arun catchment

To constrain and quantify plant wax sourcing contributed to the Arun by its tributaries, we tested four different weighting approaches. In four steps we test ecologic, climatologic, and geomorphic drivers that are all expected to influence plant wax productivity and erosive export.

The first approach assumes that plant waxes are homogeneously produced in and exported from the river catchments. Thus, we set up a function where contributions are weighted by catchment areas. We refer to this model as the *catchment-size model*:

$$p_{wax,trib}(i) = A_{trib,i}/(A_{trib,i} + A_{Arun,i-1}), \tag{5}$$

where $A_{trib,i}$ is the catchment area of all tributaries between two mainstem sites $i-1$ and i, and $A_{Arun,i-1}$ the mainstem catchment area above $i-1$.

However, because of the inhomogeneous plant cover distribution throughout individual watersheds (Figs. 1C, 2), it is likely that regions with more biomass contribute more plant wax than others. Hence, the second approach uses cumulative NPP rates to estimate plant wax derived from the Arun's tributaries. We refer to it as the *biomass model*:

$$p_{wax,trib}(i,j,k) = \sum \mathrm{NPP}_{trib,i,j} \Big/ \left(\sum \mathrm{NPP}_{Arun,i-1,k} + \sum \mathrm{NPP}_{trib,i,j}\right), \tag{6}$$

where $\sum \mathrm{NPP}_{trib,i,j}$ is the sum of j NPP rates representing all tributaries between mainstem sites $i-1$ and i and $\sum \mathrm{NPP}_{Arun,i-1,k}$ is the sum of k NPP rates within the Arun catchment above $i-1$.

In our third approach, we evaluate the role of runoff on the mobilization of organic matter. Since runoff and non-petrogenic particulate organic carbon fluxes are linked (Clark et al., 2013; Hilton et al., 2012; Schäfer et al., 2002; Smith et al., 2013; Townsend-Small et al., 2008), we weighted tributary plant wax export by cumulated rainfall. Therefore, we refer to this model as the *runoff model*:

$$p_{wax,trib}(i,j,k) = \sum \mathrm{TRMM}_{trib,i,j} \Big/ \left(\sum \mathrm{TRMM}_{Arun,i-1,k} + \sum \mathrm{TRMM}_{trib,i,j}\right), \tag{7}$$

where $p_{wax,trib}(i,j,k)$ is the relative portion of plant wax derived through all tributaries between point $i-1$ and i, and $\sum \mathrm{TRMM}_{trib,i,j}$ and $\sum \mathrm{TRMM}_{Arun,i-1,k}$ represent cumulative rainfall within all tributary pixel j between mainstem sites $i-1$ and i and of all mainstem pixel k upstream site i, respectively.

The last factor known for its effect on organic matter export is erosion (Galy et al., 2015). Erosion rates (Summerfield, 1991) and as well as erosion of organic matter (Hilton et al., 2013, 2012) have been demonstrated to relate to topographic indices, for example local relief and hill slope angle (Olen et al., 2015). Because runoff and topographic relief are not necessarily spatially consistent, we tested an additional weighting approach based on the combination of catchment relief and the *runoff model*. We refer to it as the *erosion-runoff model*:

$$p_{wax,trib}(i,j,k) = \sum \mathrm{R}\cdot\mathrm{TRMM}_{trib,i,j} \Big/ \left(\sum \mathrm{R}\cdot\mathrm{TRMM}_{Arun,i-1,k} + \sum \mathrm{R}\cdot\mathrm{TRMM}_{trib,i,j}\right), \tag{8}$$

where factors are similar to the *runoff model* (7) except that the rainfall grid was pixel-wise multiplied by local relief before weighting.

We combine the four different weighting approaches for tributary pOM export with respective approximated $\delta D_{FD,trib}$ values (4) as input parameters for a mixing model predicting $\delta D_{FD,Arun}$ values along the mainstem. The $\delta D_{FD,Arun}$ value at a mainstem site i was calculated by:

$$\delta D_{FD,Arun,i} = p_{wax,trib,i} \cdot \delta D_{FD,trib,i} + (1 - p_{wax,trib,i}) \cdot \delta D_{FD,Arun,i-1}, \quad (9)$$

where $p_{wax,trib,i}$ is the relative plant wax contribution of tributaries (fraction between 0 and 1, derived through equations (5) to (8), respectively) draining the Arun between sites $i-1$ and i. $\delta D_{FD,trib,i}$ is the estimated plant wax δD value obtained through the multi-parameter model (4), and $\delta D_{FD,Arun,i-1}$ is the Arun plant wax δD value at the upstream site $i-1$. The model start value for $\delta D_{FD,Arun,i-1}$ is the measured δD_{FD} value ($-206‰$) from the uppermost mainstem flood deposit sample at 1793 m asl. In order to allow for a potential bias of the $\delta D_{FD,Arun}$ starting value and to evaluate its effect on the model results we additionally ran the model with starting values of $-206 \pm 20‰$. Every simulation step incorporated tributaries draining the mainstem within 25 pixels alongside the DEM derived flow path of the Arun, corresponding to an average flow path length of ~2.6 km per simulation step. A detailed description of error propagation is provided in the supplement A4.

5.3.3. Estimated plant wax contributions

The evaluation of the performance of all four models is challenging, as only two downstream $\delta D_{FD,Arun}$ values are available for comparison. Nevertheless, observed trends of model results can be used in order to evaluate the model. In particular, we can test, how well the model predicts the observed isotopic difference between the lowermost and the uppermost Arun main stem sample ($\varepsilon_{HR/TP}$).

The *catchment-size model* predicted that Tibetan Plateau sources contribute 85% of plant wax yielding a $\delta D_{FD,Arun}$ value of $-202.0 \pm 0.3‰$ ($\varepsilon_{HR/TP} = 5.4 \pm 0.4‰$) at the lowermost Arun mainstem sampling location, (observed $\delta D_{FD,Arun} = -184‰$). A much smaller predicted $\varepsilon_{HR/TP}$ compared to field observations implied overestimated plant wax export from the TP and confirmed our expectation that fluvial plant wax sourcing in the Arun is not spatially uniform. The *biomass model* predicted only 41% of plant wax is sourced from the Tibetan Plateau. The predicted $\delta D_{FD,Arun}$ value was $-188.4 \pm 6.7‰$ at the lowest site with an $\varepsilon_{HR/TP}$ of $+22.5 \pm 8.4‰$ (Fig. 6B). Because of the larger uncertainties of NPP including land cover classification (Cracknell et al., 2013), leaf-surface reflectance and climate input (Zhao et al., 2006) resulting $\delta D_{FD,Arun}$ errors were much larger than for the catchment-size model. However, the *biomass model* captured the downstream $\delta D_{FD,Arun}$ value as well as the intermediate mainstem sample within prediction errors, even though tributary plant wax contributions still appear to be underestimated. But NPP may not be linearly related to the amount of exported plant waxes due to additional physical controls on mobilization and export, including catchment geomorphology and climatic conditions (Clark et al., 2013; Hilton et al., 2012; Smith et al., 2013). In order to account for export capacities, we weighted plant wax contributions by runoff, calculated from remotely-sensed rainfall. The *runoff model* predicted that 35% of plant wax in the Arun is derived from the Tibetan Plateau, and 65% originates from within the Himalayan Ranges. The modeled isotopic composition at the lowermost sample site was $-187.5 \pm 6.9‰$ with an $\varepsilon_{HR/TP}$ of $+23.6 \pm 8.6‰$, also within errors of the lowermost observed $\delta D_{FD,Arun}$ value ($-184‰$, $\varepsilon_{HR/TP} = +27.7 \pm 5‰$). Although $\delta D_{FD,Arun}$ results of the *biomass* and *runoff model* were similar at the downstream Arun mainstem site, plant wax contributions of the *biomass model* along the southern half of the transect are higher. Accordingly, *runoff-model* plant wax contributions were higher for the northern half (Fig. 6B), reflecting orographic rainout between 1.5 and 3 km asl (Figs. 1B and 2). However, both models somewhat underestimated tributary plant wax contributions along the Arun indicating the necessity of an additional parameter in order to obtain the observed $\delta D_{FD,Arun}$ pattern. The *erosion-runoff model*, accounting for erosive potential (local relief) and runoff, predicted 27% plant wax from the Tibetan plateau and 73% from the Himalaya. The $\delta D_{FD,Arun}$ value at the lowermost site was $-184.9 \pm 6.2‰$ with $\varepsilon_{HR/TP}$ of $+27.0 \pm 7.8‰$, being statistically similar to both previous models and congruent with observed downstream enrichment. Especially the intermediate sample was predicted best by the *erosion-runoff model*, indicating that a combination of runoff and erosive capacity is responsible for the export of plant wax in the Arun catchment. We note that results of the *biomass, runoff, and erosion-runoff models* are similar within prediction errors. The best fit of the *erosion-runoff model* however supports recent findings about the role of runoff and erosion on organic matter mobilization in river catchments globally (Clark et al., 2013; Galy et al., 2015; Hilton et al., 2013, 2012; Smith et al., 2013).

A sensitivity test on potentially variable $\delta D_{FD,Arun}$ starting values by taking the example of the *erosion-runoff model* yielded only small changes for a starting values of $206 \pm 20‰$: the model output for the sensitivity runs was $-189.8‰$ and $-179.4‰$, respectively, still matching the observed downstream $\delta D_{FD,Arun}$ value within the models' 95% prediction errors. This implies, that expected natural $\delta D_{FD,Arun}$ value variability of plant waxes representing the TP affects the model to a small extent only.

5.4. Implications for the plant-wax paleohydrology proxy

Our spatial sampling along a large trans-Himalayan river showed that δD values of plant waxes extracted from tributary flood deposits are representative for catchment vegetation and δD_{water} values (Fig. 4B). We found a relationship of $\delta D_{FD,trib} = 0.45^{*}\delta D_{water} - 147‰$ ($R = -0.54$, $p = 0.03$) that largely supports earlier studies showing a good correlation in fluvial deposits (Galy et al., 2011; Ponton et al., 2014) and lacustrine archives (Garcin et al., 2012; Huang et al., 2004; Polissar and Freeman, 2010; Sachse et al., 2004). Global data for annual mean precipitation and lacustrine plant wax *n*-alkane δD values (Garcin et al., 2012; Polissar and Freeman, 2010; Sachse et al., 2004) are characterized by a slightly steeper slope but comparable regression intercept $\delta D_{lakes} = 0.55^{*}\delta D_{water} + 148‰$ ($r^2 = 0.8$, $p < 0.01$). However, they are the same within the 95% confidence interval (Fig. 4B). But most calibration studies in lacustrine environments have compared surface sediment plant wax δD values to annual mean precipitation δD (Garcin et al., 2012; Polissar and Freeman, 2010; Sachse et al., 2004), which is assumed to be the source water in most contexts. We correlate $\delta D_{FD,trib}$ to post ISM surface water instead, being our best estimate of annual mean precipitation δD values. But we have to acknowledge that $\delta D_{water,trib}$ values are unlikely to precisely match plant source water δD as surface waters are affected by additional evaporation and mixing with groundwater and glacier and snow meltwater.

Whereas we confirm the link of $\delta D_{FD,trib}$ values and the isotopic composition of environmental water, our plant wax quantification approach further indicates that plant wax sourcing along the Arun is strongly biased towards tributaries with highest runoff and high erosion capacities in the forested sector of the catchment. This implies that tectonic changes on geological timescales, e.g., as a consequence of mountain range uplift, would change plant wax

source areas of fluvial deposits to the loci of erosion. Our study indicates that paleo-reconstructions based on plant wax δD data need to incorporate the effect of hydrologic and geomorphic processes on the source of these materials through changes in erosion and sediment yield.

6. Conclusions

We measured the plant wax hydrogen isotopic composition of plant leaves, river coarse particulate organic matter and flood deposits from the trans-Himalayan Arun River and tributaries in eastern Nepal. We found that plant wax *n*-alkanes in the deposits reflect the isotopic composition of modern plants in their catchments and that those plant waxes carry signatures of the elevation-related gradient in environmental waters. We use these relationships together with remote-sensing data for biomass productivity (NPP), rainfall amount, and relief to understand plant organic matter sources of fluvial deposits. Mixing models accounting for climatic, biomass, and geomorphic factors suggest that fluvial transport does not uniformly mobilize plant waxes from across the vast catchment area. Instead, sourcing is dominated by tributaries within the lowermost 15% of the catchment, draining the Arun between 205 and 1793 m river elevation. Our remote-sensing based modeling approaches demonstrated that the presence of vegetation in the Arun's tributaries is necessary for high plant organic matter export rates. However, the best fit model suggests that areas with high precipitation (and consequently high NPP) and relief dominate sourcing, emphasizing the importance of both productivity and erosion processes for plant wax exports. Our novel modeling approach provides quantitative insights into the sourcing of plant-wax biomarkers in this catchment and introduces a new interpretative framework. This framework enables robust interpretations of modern terrestrial plant biomarker sourcing and provides better constraints on the interpretation of plant wax proxy records in terms of past hydrologic changes in river catchments.

Acknowledgements

BH was funded through DFG GRK 1364 and thanks UNVEU 1966, SF through US National Science Foundation (EAR-1227192 and OCE-1401217) and the USC Women in Science and Engineering Program and DS through an Emmy-Noether grant from the German Science Foundation (DFG SA1889/1-1 and SA1889/1-2). Thanks to Manoj, Sophia Wagner and Raphael Scheffler for field assistance and Miguel Rincon, Michael Pöhle and Denise Jekel for lab assistance.

Appendix A. Supplementary material

Supplementary material related to this article can be found online at http://dx.doi.org/10.1016/j.epsl.2016.07.008. These data include the Google maps of the most important areas described in this article.

References

Andermann, C., Longuevergne, L., Bonnet, S., Crave, A., Davy, P., Gloaguen, R., 2012. Impact of transient groundwater storage on the discharge of Himalayan rivers. Nat. Geosci. 5, 127–132. http://dx.doi.org/10.1038/ngeo1356.

Bai, Y., Fang, X., Gleixner, G., Mügler, I., 2011. Effect of precipitation regime on δD values of soil *n*-alkanes from elevation gradients – implications for the study of paleo-elevation. Org. Geochem. 42, 838–845. http://dx.doi.org/10.1016/j.orggeochem.2011.03.019.

Berner, R.A., 1990. Atmospheric carbon dioxide levels over Phanerozoic time. Science 249 (4975), 1382–1386. http://dx.doi.org/10.1126/science.249.4975.1382.

Bookhagen, B., 2012. Hydrology: Himalayan groundwater. Nat. Geosci. 5, 97–98. http://dx.doi.org/10.1038/ngeo1366.

Bookhagen, B., Burbank, D.W., 2006. Topography, relief, and TRMM-derived rainfall variations along the Himalaya. Geophys. Res. Lett. 33, L08405. http://dx.doi.org/10.1029/2006GL026037.

Bookhagen, B., Burbank, D.W., 2010. Toward a complete Himalayan hydrological budget: spatiotemporal distribution of snowmelt and rainfall and their impact on river discharge. J. Geophys. Res. 115. http://dx.doi.org/10.1029/2009JF001426.

Bordet, P., 1961. Recheres géologiques dans l'Himalaya du Nepal, Région du Makalu. C.N.R.S., Paris.

Bouchez, J., Galy, V., Hilton, R.G., Gaillardet, J., Moreira-Turcq, P., Pérez, M.A., France-Lanord, C., Maurice, L., 2014. Source, transport and fluxes of Amazon River particulate organic carbon: insights from river sediment depth-profiles. Geochim. Cosmochim. Acta 133, 280–298. http://dx.doi.org/10.1016/j.gca.2014.02.032.

Burdige, D.J., 2005. Burial of terrestrial organic matter in marine sediments: a re-assessment. Glob. Biogeochem. Cycles 19, 1–7. http://dx.doi.org/10.1029/2004GB002368.

Bush, R.T., McInerney, F.A., 2013. Leaf wax *n*-alkane distributions in and across modern plants: implications for paleoecology and chemotaxonomy. Geochim. Cosmochim. Acta 117, 161–179. http://dx.doi.org/10.1016/j.gca.2013.04.016.

Carpenter, C., Zomer, R., 1996. Forest ecology of the Makalu–Barun National Park and Conservation Area, Nepal. Mt. Res. Dev. 16, 135–148. http://dx.doi.org/10.2307/3674007.

Clark, K.E., Hilton, R.G., West, A.J., Malhi, Y., Gröcke, D.R., Bryant, C.L., Ascough, P.L., Robles Caceres, A., New, M., 2013. New views on "old" carbon in the Amazon River: insight from the source of organic carbon eroded from the Peruvian Andes. Geochem. Geophys. Geosyst. 14, 1644–1659. http://dx.doi.org/10.1002/ggge.20122.

Cracknell, A.P., Kanniah, K.D., Tan, K.P., Wang, L., 2013. Evaluation of MODIS gross primary productivity and land cover products for the humid tropics using oil palm trees in Peninsular Malaysia and Google Earth imagery. Int. J. Remote Sens. 34, 7400–7423. http://dx.doi.org/10.1080/01431161.2013.820367.

Dansgaard, W., 1964. Stable isotopes in precipitation. Tellus 16, 436–468. http://dx.doi.org/10.3402/tellusa.v16i4.8993.

Dobremez, J., Shakya, P., 1975. Carte Ecologique du Népal. VI. Region Biratnagar–Kanchenjunga 1:250,000. Doc. Cartogr. Ecol. XVI, 33–46.

Ernst, N., Peterse, F., Breitenbach, S.F.M., Syiemlieh, H.J., Eglinton, T.I., 2013. Biomarkers record environmental changes along an altitudinal transect in the wettest place on Earth. Org. Geochem. 60, 93–99. http://dx.doi.org/10.1016/j.orggeochem.2013.05.004.

Feakins, S.J., Sessions, A.L., 2010. Controls on the D/H ratios of plant leaf waxes in an arid ecosystem. Geochim. Cosmochim. Acta 74, 2128–2141. http://dx.doi.org/10.1016/j.gca.2010.01.016.

France-Lanord, C., Derry, L., 1997. Organic carbon burial forcing of the carbon cycle from Himalayan erosion. Nature 390, 65–67. http://dx.doi.org/10.1038/36324.

Freeman, K.H., Colarusso, L.A., 2001. Molecular and isotopic records of C_4 grassland expansion in the late miocene. Geochim. Cosmochim. Acta 65, 1439–1454. http://dx.doi.org/10.1016/S0016-7037(00)00573-1.

Galy, V., Eglinton, T., 2011. Protracted storage of biospheric carbon in the Ganges–Brahmaputra basin. Nat. Geosci. 4, 843–847. http://dx.doi.org/10.1038/ngeo1293.

Galy, V., Eglinton, T., France-Lanord, C., Sylva, S., 2011. The provenance of vegetation and environmental signatures encoded in vascular plant biomarkers carried by the Ganges–Brahmaputra rivers. Earth Planet. Sci. Lett. 304, 1–12. http://dx.doi.org/10.1016/j.epsl.2011.02.003.

Galy, V., Peucker-Ehrenbrink, B., Eglinton, T., 2015. Global carbon export from the terrestrial biosphere controlled by erosion. Nature 521, 204–207. http://dx.doi.org/10.1038/nature14400.

Garcin, Y., Schwab, V.F., Gleixner, G., Kahmen, A., Todou, G., Séné, O., Onana, J.-M., Achoundong, G., Sachse, D., 2012. Hydrogen isotope ratios of lacustrine sedimentary *n*-alkanes as proxies of tropical African hydrology: insights from a calibration transect across Cameroon. Geochim. Cosmochim. Acta 79, 106–126. http://dx.doi.org/10.1016/j.gca.2011.11.039.

Garzione, C.N., Quade, J., DeCelles, P.G., English, N.B., 2000. Predicting paleoelevation of Tibet and the Himalaya from δ^{18}O vs. altitude gradients in meteoric water across the Nepal Himalaya. Earth Planet. Sci. Lett. 183, 215–229. http://dx.doi.org/10.1016/S0012-821X(00)00252-1.

Gonfiantini, R., Roche, M.A., Olivry, J.C., Fontes, J.C., Zuppi, G.M., 2001. The altitude effect on the isotopic composition of tropical rains. Chem. Geol. 181, 147–167. http://dx.doi.org/10.1016/S0009-2541(01)00279-0.

Goñi, M.A., Moore, E., Kurtz, A., Portier, E., Alleau, Y., Merrell, D., 2014. Organic matter compositions and loadings in soils and sediments along the Fly River, Papua New Guinea. Geochim. Cosmochim. Acta 140, 275–296. http://dx.doi.org/10.1016/j.gca.2014.05.034.

Goñi, M., Ruttenberg, K., Eglinton, T., 1997. Sources and contribution of terrigenous organic carbon to surface sediments in the Gulf of Mexico. Nature 389, 275–278.

Goñi, M.A., Yunker, M.B., MacDonald, R.W., Eglinton, T.I., 2000. Distribution and sources of organic biomarkers in arctic sediments from the Mackenzie River and Beaufort Shelf. Mar. Chem. 71, 23–51. http://dx.doi.org/10.1016/S0304-4203(00)00037-2.

Hatten, J.A., Goñi, M.A., Wheatcroft, R.A., 2012. Chemical characteristics of particulate organic matter from a small, mountainous river system in the Oregon Coast Range, USA. Biogeochemistry 107, 43–66. http://dx.doi.org/10.1007/s10533-010-9529-z.

Hedges, J.I., Clark, W.A., Quay, P.D., Richey, J.E., Devol, A.H., Santos, U.D.M., 1986. Compositions and fluxes of particulate organic material in the Amazon River. Limnol. Oceanogr. 31, 717–738. http://dx.doi.org/10.4319/lo.1986.31.4.0717.

Hedges, J.I., Cowie, G.L., Richey, J.E., Quay, P.D., Benner, R., Strom, M., Forsberg, B.R., 1994. Origins and processing of organic matter in the Amazon River as indicated by carbohydrates and amino acids. Limnol. Oceanogr. 39, 743–761. http://dx.doi.org/10.4319/lo.1994.39.4.0743.

Hedges, J.I., Mayorga, E., Tsamakis, E., McClain, M.E., Aufdenkampe, A., Quay, P., Richey, J.E., Benner, R., Opsahl, S., Black, B., 2000. Organic matter in Bolivian tributaries of the Amazon River: a comparison to the lower mainstream. Limnol. Oceanogr. 45, 1449–1466. http://dx.doi.org/10.4319/lo.2000.45.7.1449.

Hilton, R.G., Galy, A., Hovius, N., Kao, S.-J., Horng, M.-J., Chen, H., 2012. Climatic and geomorphic controls on the erosion of terrestrial biomass from subtropical mountain forest. Glob. Biogeochem. Cycles 26. http://dx.doi.org/10.1029/2012GB004314.

Hilton, R.G., Galy, A., West, A.J., Hovius, N., Roberts, G.G., 2013. Geomorphic control on the δ^{15}N of mountain forests. Biogeosciences 10, 1693–1705. http://dx.doi.org/10.5194/bg-10-1693-2013.

Hoffmann, B., Kahmen, A., Cernusak, L.A., Arndt, S.K., Sachse, D., 2013. Abundance and distribution of leaf wax *n*-alkanes in leaves of acacia and eucalyptus trees along a strong humidity gradient in Northern Australia. Org. Geochem. 62, 62–67. http://dx.doi.org/10.1016/j.orggeochem.2013.07.003.

Hou, J., D'Andrea, W.J., MacDonald, D., Huang, Y., 2007. Hydrogen isotopic variability in leaf waxes among terrestrial and aquatic plants around Blood Pond, Massachusetts (USA). Org. Geochem. 38, 977–984. http://dx.doi.org/10.1016/j.orggeochem.2006.12.009.

Hren, M.T., Bookhagen, B., Blisniuk, P.M., Booth, A.L., Chamberlain, C.P., 2009. δ^{18}O and δD of streamwaters across the Himalaya and Tibetan Plateau: implications for moisture sources and paleoelevation reconstructions. Earth Planet. Sci. Lett. 288, 20–32. http://dx.doi.org/10.1016/j.epsl.2009.08.041.

Huang, Y., Shuman, B., Wang, Y., Webb, T., 2004. Hydrogen isotope ratios of individual lipids in lake sediments as novel tracers of climatic and environmental change: a surface sediment test. J. Paleolimnol. 31, 363–375. http://dx.doi.org/10.1023/B:JOPL.0000021855.80535.13.

Huffman, G.J., Bolvin, D.T., Nelkin, E.J., Wolff, D.B., Adler, R.F., Gu, G., Hong, Y., Bowman, K.P., Stocker, E.F., 2007. The TRMM Multisatellite Precipitation Analysis (TMPA): quasi-global, multiyear, combined-sensor precipitation estimates at fine scales. J. Hydrometeorol. 8, 38–55. http://dx.doi.org/10.1175/JHM560.1.

Jessup, M.J., Newell, D.L., Cottle, J.M., Berger, A.L., Spotila, J.A., 2008. Orogen-parallel extension and exhumation enhanced by denudation in the trans-Himalayan Arun River gorge, Ama Drime Massif, Tibet–Nepal. Geology 36, 587. http://dx.doi.org/10.1130/G24722A.1.

Jia, G., Wei, K., Chen, F., Peng, P., 2008. Soil *n*-alkane δD vs. altitude gradients along Mount Gongga, China. Geochim. Cosmochim. Acta 72, 5165–5174. http://dx.doi.org/10.1016/j.gca.2008.08.004.

Kahmen, A., Hoffmann, B., Schefuß, E., Arndt, S.K., Cernusak, L.A., West, J.B., Sachse, D., 2013a. Leaf water deuterium enrichment shapes leaf wax *n*-alkane δD values of angiosperm plants II: observational evidence and global implications. Geochim. Cosmochim. Acta 111, 50–63. http://dx.doi.org/10.1016/j.gca.2012.09.004.

Kahmen, A., Schefuß, E., Sachse, D., 2013b. Leaf water deuterium enrichment shapes leaf wax *n*-alkane δD values of angiosperm plants I: experimental evidence and mechanistic insights. Geochim. Cosmochim. Acta 111, 39–49. http://dx.doi.org/10.1016/j.gca.2012.09.003.

Kao, S.-J., Liu, K.-K., 1996. Particulate organic carbon export from a subtropical mountainous river (Lanyang Hsi) in Taiwan. Limnol. Oceanogr. 41, 1749–1757. http://dx.doi.org/10.4319/lo.1996.41.8.1749.

Kim, J.H., Zell, C., Moreira-Turcq, P., Pérez, M.A.P., Abril, G., Mortillaro, J.M., Weijers, J.W.H., Meziane, T., Sinninghe Damsté, J.S., 2012. Tracing soil organic carbon in the lower Amazon River and its tributaries using GDGT distributions and bulk organic matter properties. Geochim. Cosmochim. Acta 90, 163–180. http://dx.doi.org/10.1016/j.gca.2012.05.014.

Lang, T.J., Barros, A.P., 2004. Winter storms in the Central Himalayas. J. Meteorol. Soc. Jpn. 82, 829–844. http://dx.doi.org/10.2151/jmsj.2004.829.

Olen, S.M., Bookhagen, B., Hoffmann, B., Sachse, D., Adhikari, D.P., Strecker, M.R., 2015. Understanding erosion rates in the Himalayan orogen: a case study from the Arun Valley. J. Geophys. Res., Earth Surf. 120, 2080–2102. http://dx.doi.org/10.1002/2014JF003410.

Peterse, F., van der Meer, M.T.J., Schouten, S., Jia, G., Ossebaar, J., Blokker, J., Sinninghe Damsté, J.S., 2009. Assessment of soil *n*-alkane δD and branched tetraether membrane lipid distributions as tools for paleoelevation reconstruction. Biogeosci. Discuss. 6, 2799–2807. http://dx.doi.org/10.5194/bgd-6-8609-2009.

Polissar, P.J., Freeman, K.H., 2010. Effects of aridity and vegetation on plant-wax δD in modern lake sediments. Geochim. Cosmochim. Acta 74, 5785–5797. http://dx.doi.org/10.1016/j.gca.2010.06.018.

Ponton, C., West, A.J., Feakins, S.J., Galy, V., 2014. Leaf wax biomarkers in transit record river catchment composition. Geophys. Res. Lett. 41, 6420–6427. http://dx.doi.org/10.1002/2014GL061328.Received.

Quade, J., English, N., DeCelles, P.G., 2003. Silicate versus carbonate weathering in the Himalaya: a comparison of the Arun and Seti River watersheds. Chem. Geol. 202, 275–296. http://dx.doi.org/10.1016/j.chemgeo.2002.05.002.

Rowley, D.B., Garzione, C.N., 2007. Stable isotope-based paleoaltimetry. Annu. Rev. Earth Planet. Sci. 35, 463–508. http://dx.doi.org/10.1146/annurev.earth.35.031306.140155.

Rowley, D.B., Pierrehumbert, R.T., Currie, B.S., 2001. A new approach to stable isotope-based paleoaltimetry: implications for paleoaltimetra and paleohypsometry of the High Himalaya since the Late Miocene. Earth Planet. Sci. Lett. 5836, 1–17.

Running, S.W., Nemani, R.R., Heinsch, F.A., Zhao, M., Reeves, M., Hashimoto, H., 2004. A continuous satellite-derived measure of global terrestrial primary production. Bioscience 54, 547. http://dx.doi.org/10.1641/0006-3568(2004)054[0547:ACSMOG]2.0.CO;2.

Sachse, D., Radke, J., Gleixner, G., 2004. Hydrogen isotope ratios of recent lacustrine sedimentary *n*-alkanes record modern climate variability. Geochim. Cosmochim. Acta 68, 4877–4889. http://dx.doi.org/10.1016/j.gca.2004.06.004.

Sachse, D., Radke, J., Gleixner, G., 2006. δD values of individual *n*-alkanes from terrestrial plants along a climatic gradient – implications for the sedimentary biomarker record. Org. Geochem. 37, 469–483. http://dx.doi.org/10.1016/j.orggeochem.2005.12.003.

Schäfer, J., Blanc, G., Lapaquellerie, Y., Maillet, N., Maneux, E., Etcheber, H., 2002. Ten-year observation of the Gironde tributary fluvial system: fluxes of suspended matter, particulate organic carbon and cadmium. Mar. Chem. 79, 229–242. http://dx.doi.org/10.1016/S0304-4203(02)00066-X.

Schefuß, 2003. African vegetation controlled by tropical sea surface temperatures in the mid-Pleistocene period. Nature 422, 418–421. http://dx.doi.org/10.1038/nature01500.

Schlünz, B., Schneider, R.R., 2000. Transport of terrestrial organic carbon to the oceans by rivers: re-estimating flux and burial rates. Int. J. Earth Sci. 88, 599–606. http://dx.doi.org/10.1007/s005310050290.

Schwanghart, W., Kuhn, N.J., 2010. TopoToolbox: a set of Matlab functions for topographic analysis. Environ. Model. Softw. 25, 770–781. http://dx.doi.org/10.1016/j.envsoft.2009.12.002.

Smith, J.C., Galy, A., Hovius, N., Tye, A.M., Turowski, J.M., Schleppi, P., 2013. Runoff-driven export of particulate organic carbon from soil in temperate forested uplands. Earth Planet. Sci. Lett. 365, 198–208. http://dx.doi.org/10.1016/j.epsl.2013.01.027.

Stocklin, J., 1980. Geology of Nepal and its regional frame: thirty-third William Smith lecture. J. Geol. Soc. (Lond.) 137, 1–34. http://dx.doi.org/10.1144/gsjgs.137.1.0001.

Summerfield, M.A., 1991. Global Geomorphology: An Introduction to the Study of Landforms. Longman Scientific & Technical, Harlow, Essex, England.

Tao, S., Eglinton, T.I., Montluçon, D.B., McIntyre, C., Zhao, M., 2015. Pre-aged soil organic carbon as a major component of the Yellow River suspended load: regional significance and global relevance. Earth Planet. Sci. Lett. 414, 77–86. http://dx.doi.org/10.1016/j.epsl.2015.01.004.

Tierney, J.E., Russell, J.M., Huang, Y., Sinninghe Damsté, J.S., Hopmans, E.C., Cohen, A.S., 2008. Northern hemisphere controls on tropical southeast African climate during the past 60,000 years. Science 322 (5899), 252–255. http://dx.doi.org/10.1126/science.1160485.

Tipple, B.J., Pagani, M., 2013. Environmental control on eastern broadleaf forest species' leaf wax distributions and D/H ratios. Geochim. Cosmochim. Acta 111, 64–77. http://dx.doi.org/10.1016/j.gca.2012.10.042.

Townsend-Small, A., McClain, M.E., Hall, B., Noguera, J.L., Llerena, C.A., Brandes, J.A., 2008. Suspended sediments and organic matter in mountain headwaters of the Amazon River: results from a 1-year time series study in the central Peruvian Andes. Geochim. Cosmochim. Acta 72, 732–740. http://dx.doi.org/10.1016/j.gca.2007.11.020.

USGS, 2006. Shuttle Radar Topography Mission, 3 Arc Second Scene. Global Land Cover Facility. University of Maryland, College Park, MD.

Wan, Z., Dozier, J., 1996. A generalized split-window algorithm for retrieving land-surface temperature from space. IEEE Trans. Geosci. Remote Sens. 34, 892–905. http://dx.doi.org/10.1109/36.508406.

Weijers, J.W.H., Schouten, S., Schefuß, E., Schneider, R.R., Sinninghe Damsté, J.S., 2009. Disentangling marine, soil and plant organic carbon contributions to continental margin sediments: a multi-proxy approach in a 20,000 year sediment record from the Congo deep-sea fan. Geochim. Cosmochim. Acta 73, 119–132. http://dx.doi.org/10.1016/j.gca.2008.10.016.

West, A.J., Lin, C.-W., Lin, T.-C., Hilton, R.G., Liu, S.-H., Chang, C.-T., Lin, K.-C., Galy, A., Sparkes, R.B., Hovius, N., 2011. Mobilization and transport of coarse woody debris to the oceans triggered by an extreme tropical storm. Limnol. Oceanogr. 56, 77–85. http://dx.doi.org/10.4319/lo.2011.56.1.0077.

Wheatcroft, R.A., Goñi, M.A., Hatten, J.A., Pasternack, G.B., Warrick, J.A., 2010. The role of effective discharge in the ocean delivery of particulate organic carbon by small, mountainous river systems. Limnol. Oceanogr. 55, 161–171. http://dx.doi.org/10.4319/lo.2010.55.1.0161.

Zhao, M., Running, S.W., Nemani, R.R., 2006. Sensitivity of Moderate Resolution Imaging Spectroradiometer (MODIS) terrestrial primary production to the accuracy of meteorological reanalyses. J. Geophys. Res., Biogeosci. 111, 1–13. http://dx.doi.org/10.1029/2004JG000004.